3D Face Matching and Registration Based on Hyperbolic Ricci Flow

Wei Zeng[213] Xiaotian Yin[1] Yun Zeng[1] Yukun Lai[1] Xianfeng Gu[1] Dimitris Samaras[1]

[1]Computer Science Department, Stony Brook University, NY USA
[2]Institute of Computing Technology, Chinese Academy of Sciences
[3]Graduate School of Chinese Academy of Science

{zengwei, xyin, yzeng, ylai, gu, samaras}@cs.sunysb.edu

Abstract

3D surface matching is fundamental for shape analysis. As a powerful method in geometric analysis, Ricci flow can flexibly design metrics by prescribed target curvature. In this paper we describe a novel approach for matching surfaces with complicated topologies based on hyperbolic Ricci flow. For surfaces with negative Euler characteristics, such as a human face with holes (eye contours), the canonical hyperbolic metric is conformal to the original and can be efficiently computed. Then the surface can be canonically decomposed to hyperbolic hexagons. By matching the corresponding hyperbolic hexagons, the matching between surfaces can be easily established. Compared to existing methods, hyperbolic Ricci flow induces diffeomorphisms between surfaces with complicated topologies with negative Euler characteristics, while avoiding singularities. Furthermore, all the boundaries are intrinsically mapped to hyperbolic lines as alignment constraints. Finally, we demonstrate the applicability of this intrinsic shape representation for 3D face matching and registration.

1. Introduction

In recent decades, there has been a lot of research into surface representations for 3D surface analysis, which is a fundamental issue for many computer vision applications, such as 3D shape registration, partial scan alignment, 3D object recognition, and classification [5, 15, 25, 35]. In particular, as 3D scanning technologies improve, large databases of 3D scans require automated methods for matching and registration. However, matching surfaces undergoing non-rigid deformation is still a challenging problem, especially when data is noisy and with complicated topology. Different approaches include curvature-based representations [31, 36], regional point representations [25, 29], spherical harmonic representations [8, 9], shape distributions [24], multi-dimensional scaling[3, 4], local isometric mapping [28], summation invariants [21], landmark-sliding [7], physics-based deformable models [30], Free-Form Deformation (FFD) [14], and Level-Set based methods [23]. However, many surface representations that use local geometric invariants can not guarantee a global convergence and might suffer from local minima in the presence of non-rigid deformations. To address this issue, many global parameterization methods have been developed recently based on conformal geometric maps [37, 20, 11, 27, 33, 34, 32]. Although the previous methods have met with a great deal of success in both computer vision and graphics, there are two major shortcomings in conformal maps when applied to matching of real discrete data such as the output of 3D scanners: 1) *complicated topology of the inputs*, and 2) *singularities of the conformal maps*. In this paper we will address the above two issues by introducing a novel algorithm for multiply connected surfaces based on hyperbolic Ricci flow [18].

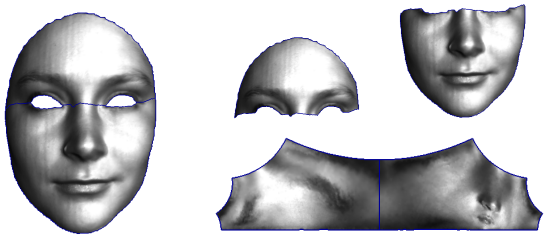

Figure 1. Hyperbolic hexagon decomposition.

Most existing conformal mapping methods can only handle surfaces with the simplest topology, namely, genus zero surface with a single boundary. In reality, due to partial occlusion, noise, an arbitrary surface patch acquired by a single scan by a camera-based 3D scanner, eg. face frontal scan, cloth, machine parts etc, is a genus zero surface with arbitrary number of holes, which are called multiply connected domains and have negative Euler characteristic number $\chi = 2 - 2g - b$, where g is the number of genus and b is the number of boundaries. For a human face with two eyes open, $\chi = -1$, where $g = 0$, $b = 3$. The only pre-

vious existing conformal geometric method that can handle such surfaces is the Euclidean Ricci Flow (ERF) method in [17, 16, 10]. ERF is globally one-to-one but has singularities whose placement affects the area distortion of discrete conformal mapping greatly [12, 19, 10, 16]. Other methods, such as harmonic maps [34] and Least-Squares Conformal Maps (LSCMs) [20], are not guaranteed to generate diffeomorphisms between multiply connected domains.

According to conformal geometry, for surfaces with negative Euler characteristic number such as a human face with multiple holes, there exists a unique Riemannian metric, such that the boundaries are geodesics, and each interior point has constant -1 Gaussian curvature. Such a metric is called *the hyperbolic uniformization metric* [18, 16]. The Hyperbolic uniformization metric is conformal to the metric of the surface. Such conformal maps are called *hyperbolic conformal maps*. By using this powerful tool, Hyperbolic Ricci Flow (HRF) [18], the canonical hyperbolic metric can be efficiently computed. Then the surface can be canonically decomposed to hyperbolic hexagons, which are embedded in the hyperbolic space. The boundaries of the hexagons are hyperbolic lines, so they are intrinsic to the surface and the alignment of boundaries can be enforced during matching. By matching the corresponding hyperbolic hexagons, the mapping between surfaces can be easily established.

In this work, we applied hyperbolic conformal maps and hyperbolic hexagon decomposition for surface matching. Figure 1 gives an example, where a human face surface is decomposed to 2 parts by 3 geodesics between each two boundaries and each part is mapped to a hyperbolic hexagon. Hyperbolic conformal maps by hyperbolic Ricci flow method have no singularity, and can be efficiently used for matching surfaces with complicated topology, without any restriction on the number of holes. In the hyperbolic representation, all boundaries are mapped to hyperbolic lines, which facilitates boundary alignment.

The rest of the paper is organized as follows: the theoretic background is introduced in Section 2. The algorithm for the hyperbolic mapping of genus zero surfaces with complicated topology using discrete hyperbolic Ricci flow is described in Section 3. The algorithms for 3D surface matching and canonical segmentation are proposed in Section 4. Experiments are presented in Section 5, and we conclude with discussion and future work in Section 6.

2. Theoretic Background

Here, we introduce the basic theoretic concepts. For more details, we refer readers to [12, 17, 18, 16].

Riemannian Metric Suppose S is a surface embedded in the Euclidean space $\mathbb{R}^3$, its first fundamental form is called the Riemannian metric, which is represented as a tensor $\mathbf{g} = (g_{ij})$. A metric defines an inner product for the tangent vectors. Suppose two tangent vectors $\mathbf{v}_1 = (du_1, dv_1), \mathbf{v}_2 = (du_2, dv_2)$ are on the tangent plane at a point $p \in S$, then their inner product is defined as

$$< \mathbf{v}_1, \mathbf{v}_2 >_{\mathbf{g}} = \sum_{ij} g_{ij} du_i dv_j.$$

The angle between $\mathbf{v}_1, \mathbf{v}_2$ measured by $\mathbf{g}$ is given by

$$\theta_{\mathbf{g}} = cos^{-1} \frac{< \mathbf{v}_1, \mathbf{v}_2 >_{\mathbf{g}}}{\sqrt{< \mathbf{v}_1, \mathbf{v}_1 >_{\mathbf{g}} < \mathbf{v}_2, \mathbf{v}_2 >_{\mathbf{g}}}} \tag{1}$$

Suppose $\bar{g}$ is another Riemannian metric on S, if

$$\bar{\mathbf{g}} = e^{2\lambda} \mathbf{g},$$

where λ is a function. Then we say $\bar{\mathbf{g}}$ is conformal to $\mathbf{g}$. Using Eqn. 1, we can show that for all angles between two tangent vectors, $\theta_{\mathbf{g}} = \theta_{\bar{\mathbf{g}}}$. λ measures the area distortion and called *conformal factor*.

Uniformization Metric Suppose S is a surface embedded in the Euclidean space $\mathbb{R}^3$ with negative Euler characteristic numbers $\chi(S) < 0$. Then S has an induced Euclidean metric $\mathbf{g} = \{g_{ij}\}$. The Gaussian curvature K of the interior point and the geodesic curvature of the boundary point on the surface are determined by the metric $\mathbf{g}$. The total curvature satisfies the Gauss-Bonnet theorem:

$$\int_S K dA + \int_{\partial S} k_g ds = 2\pi\chi(S), \tag{2}$$

where ∂S represents the boundary of the surface and is non empty, dA the area element, and dS the length element. According to the Riemann uniformization theorem [16], there exists a unique Riemannian metric $\bar{\mathbf{g}}$, such that $\bar{\mathbf{g}}$ is conformal to $\mathbf{g}$, $\bar{\mathbf{g}} = e^{2u}\mathbf{g}$. The Gaussian curvature induced by $\bar{\mathbf{g}}$ equals to -1 everywhere and the geodesic curvature $\bar{k}_g$ equals to 0. Such a metric is called the *uniformization metric* of S.

Ricci Flow Ricci flow is a powerful curvature flow method, invented by Hamilton for the proof of the Poincaré conjecture [13]. Intuitively, Ricci flow is the process to deform the Riemannian metric according to the curvature, such that the curvature evolves like a heat diffusion process.

$$\frac{dg_{ij}}{dt} = -2K + \frac{\chi(S)}{A}, \tag{3}$$

where K is the Gaussian curvature induced by the metric $\mathbf{g}(t)$, A is the area of the surface. For surfaces with non-positive Euler numbers, Hamilton proved the convergence of Ricci flow in [13]:

Theorem 2.1 (Hamilton 1988) *For a closed surface of non-positive Euler characteristic, if the total area of the surface is preserved during the flow, the Ricci flow will converge to a metric such that the Gaussian curvature is constant every where.*

In our work, we compute the hyperbolic uniformization metric using the surface Ricci flow method.

3. Discrete Hyperbolic Ricci Flow

In this section, we introduce the conformal mapping using discrete hyperbolic Ricci flow and refer readers to [18, 16] for detailed discussion.

Hyperbolic Geometry Most computation in this work is carried out in the background of hyperbolic geometry. Here, we briefly introduce the elementary concepts in hyperbolic geometry. The Hyperbolic space $\mathbb{H}^2$ can not be realized in $\mathbb{R}^3$, instead we use the following Poincaré model to represent it. The Poincaré disk is the unit disk on the complex plane $|z| < 1, z = x + iy$, with Riemannian metric

$$ds^2 = \frac{4dzd\bar{z}}{(1-\bar{z}z)^2}.$$

The *rigid motion* in the hyperbolic space is a Möbius transformation

$$z \to \exp^{i\theta} \frac{z - z_0}{1 - \bar{z}_0 z}$$

A *hyperbolic line* (a geodesic) is a circular arc, which is orthogonal to the unit circle $|z| = 1$. A *hyperbolic circle* (c, r) (where c is the center, r is the radius) looks like a Euclidean circle (C, R), where

$$C = \frac{2 - 2\mu^2}{1 - \mu^2|c|^2}, R^2 = |C|^2 - \frac{|c|^2 - \mu^2}{1 - \mu^2|c|^2},$$

where $\mu = \frac{e^r - 1}{e^r + 1}$, as shown in Figure 2.

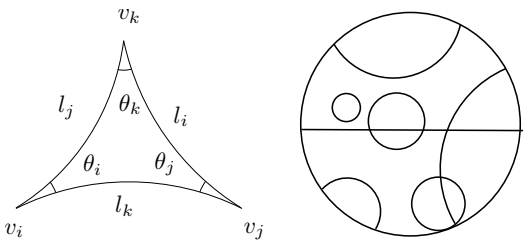

Figure 2. Hyperbolic triangle, lines and circles.

There are other models of hyperbolic space. Another commonly used one is the *Klein model* [18]. The Klein model is also the unit disk, all geodesics are straight Euclidean lines, this fact greatly simplifies the processing. The conversion from the Poincaré disk to the Klein model is straightforward:

$$z \to \frac{2z}{1 + \bar{z}z}. \tag{4}$$

The Poincaré model is conformal, whereas Klein model is not.

Hyperbolic Ricci Flow In practice, all surfaces are approximated by triangular meshes. Let M be a triangular mesh, $\{v_1, v_2, \cdots, v_n\}$ be the vertex set, $[v_i, v_j]$ be an edge connecting v_i and v_j, $[v_i, v_j, v_k]$ be a face. Then the *discrete metric* of M is the edge lengths. Let θ_i^{jk} be the corner angle at vertex v_i in the face $[v_i, v_j, v_k]$. We treat each face $[v_i, v_j, v_k]$ as a hyperbolic triangle, therefore θ_i^{jk} is determined by the edge lengths using hyperbolic cosine law. The *discrete Gaussian curvature* is defined as the angle deficit,

$$K_i = \begin{cases} 2\pi - \sum \theta_i^{jk} & v_i \notin \partial M \\ \pi - \sum \theta_i^{jk} & v_i \in \partial M \end{cases}.$$

We define circle packing metric on M in the following way.

Definition 3.1 (Circle Packing Metric) *Let M be a triangular mesh. We associate each vertex v_i with a disk with radius γ_i. On edge $e_{ij} = [v_i, v_j]$, the two circles intersect at the angle ϕ_{ij}. Then the edge length l_{ij} of e_{ij} is determined by the hyperbolic cosine law:*

$$\cosh l_{ij} = \cosh \gamma_i \cosh \gamma_j + \sinh \gamma_i \sinh \gamma_j \cos \phi_{ij}. \tag{5}$$

A circle packing metric is denoted as (M, Γ, Φ), where $\Gamma : v_i \to \gamma_i$ represents the radius, $\Phi : e_{ij} \to \phi_{ij}$ represents the intersection angle. See Figure 3.

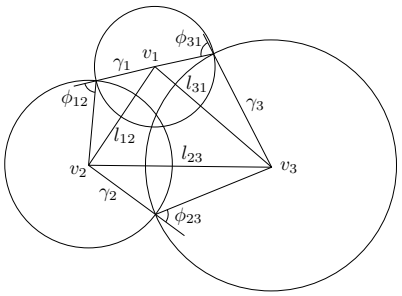

Figure 3. Circle packing metric.

Then the discrete hyperbolic Ricci flow is defined as:

Definition 3.2 (Hyperbolic Ricci Flow) *Let $u_i = \log \tanh \frac{\gamma_i}{2}$, $\mathbf{u} = (u_1, u_2, \cdots, u_n)$, then the discrete Ricci flow is defined as*

$$\frac{du_i(t)}{dt} = -K_i, \tag{6}$$

where K_i is the discrete Gaussian curvature at v_i.

The convergence of the discrete hyperbolic Ricci flow is proven by Chow and Luo [6]:

Theorem 3.3 (Convergence) *A hyperbolic discrete Ricci flow converges, furthermore the convergence is exponentially fast,*

$$|K_i(t) - \bar{K}_i| < c_1 \exp^{-c_2 t},$$

and

$$|\gamma_i(t) - \bar{\gamma}_i| < c_1 \exp^{-c_2 t},$$

where c_1 and c_2 are two positive constants.

Furthermore, we can show that the discrete Ricci flow is the negative gradient flow of the following Ricci energy [6].

Definition 3.4 (Ricci Energy) *The Ricci energy for circle packing metric (M, Γ, Φ) is defined as*

$$E(\mathbf{u}) = \int_{\mathbf{u}_0}^{\mathbf{u}} \sum_{i=1}^{n} (\bar{K}_i - K_i) du_i, \tag{7}$$

where $\mathbf{u}_0 = (0, 0, \cdots, 0)$.

Theorem 3.5 (Hyperbolic Ricci Energy) *The discrete hyperbolic Ricci energy is convex. It has a unique global minimum, which induces the target curvature $\bar{K}_i$.*

Therefore, in order to compute the uniformization metric, we can set the target curvature $\bar{K}_i \equiv 0$ for all vertices, and optimize the Ricci energy using Newton's method. The Hessian matrix of the Ricci energy can be easily computed by

$$\frac{\partial^2 E(\mathbf{u})}{\partial u_i \partial u_j} = -\frac{\partial K_i}{\partial u_j}.$$

4. Algorithm for Surface Matching

Suppose S_1 and S_2 are two given surfaces, then our goal is to find an one to one map $f : S_1 \to S_2$, which is as close to an isometry as possible. Instead of matching the two surfaces in $\mathbb{R}^3$ directly, we find two conformal maps $\phi_k : S_k \to D_k, k = 1, 2$ which map the surface to the planar domains D_k, then we compute a planar map between the planar domains $\tilde{f} : D_1 \to D_2$. Then the matching is the composition $f = \phi_2^{-1} \circ \tilde{f} \circ \phi_1$.

$$\begin{array}{ccc} S_1 & \xrightarrow{f} & S_2 \\ {\scriptstyle \phi_1}\downarrow & & \downarrow{\scriptstyle \phi_2} \\ D_1 & \xrightarrow{\tilde{f}} & D_2 \end{array}$$

In theory, if f is isometric and the boundary conditions are consistently set, then $\tilde{f}$ is an identity. In our applications for 3D face matching, the mappings are close to isometry [1]. Therefore, the planar mappings are near to the identities. This greatly simplifies the matching process.

Through the hyperbolic mapping, each open surface with two holes can be decomposed to 2 hyperbolic hexagons, H_1, H_2, as shown in Figure 1. In practice, it is often useful to add feature constraints, such as point and curve correspondences when comparing 3D shapes. Since the boundaries of hyperbolic hexagons are geodesics, it is intrinsic to enforce the corresponding geodesics to be matched.

The general algorithm pipeline is as follows:

1. Compute the uniformization metric using discrete hyperbolic Ricci flow.

2. Flatten the surface with the hyperbolic metric onto the Poincaré model.

3. Segment the surface with the hyperbolic metric to canonical hyperbolic hexagons along geodesics on the planar image, which form the planar domain D.

4. Build the mapping between hyperbolic hexagons and construct the mapping between the original surfaces.

Step 1 has been explained in the last section. In the following subsections, we explain each step in details.

4.1. Flattening the Surface

Once the hyperbolic metric has been computed, we can flatten the surface isometrically onto the Poincaré disk [18, 16].

1. Suppose a hyperbolic triangle has edge lengths $\{l_i, l_j, l_k\}$, then we compute the angle θ_k using the hyperbolic cosine law of Eqn. 5.

2. Set the coordinates of v_k to 0, those of v_i to $\cosh \frac{l_j}{2}$, those of v_j to $e^{i\theta_k} \cosh \frac{l_i}{2}$.

3. Glue the planar images of adjacent triangles by Möbius transformations. Suppose $f_1 = [v_i, v_j, v_k]$ and $f_2 = [v_j, v_i, v_l]$ are two adjacent triangles, the planar complex coordinates of v_i, v_j, v_k are z_i, z_j, z_k. We construct a Möbius transformation $\phi_1 : f_1 \to D$, such that $\phi_1(z_i)$ is the origin, $\phi_1(z_j)$ is on the real axis. ϕ_1

$$\tau_1 : z \to \frac{z - z_i}{1 - \bar{z}_i z},$$

then τ_1 maps z_i to 0, maps edge $[v_i, v_j]$ to a straight line. Then we construct another Möbius transformation

$$\tau_2 : z \to e^{i\theta} z,$$

where $\theta = arg \tau_1(z_j)$. Let $\phi_1 = \tau_2 \circ \tau_1 : f_1 \to D$, then ϕ_1 maps v_i to the origin, ϕ_1 maps v_j to be on the real axis. Similarly, we construct $\phi_2 : f_2 \to D$, which maps v_i to the origin, and v_j to be on the real axis. Then the Möbius transformation $\phi_2^{-1} \circ \phi_1$ glues the planar image of f_2 to the planar image of f_1 along edge $[v_i, v_j]$.

The improvements of computational accuracy for hyperbolic flattening have been discussed in [16].

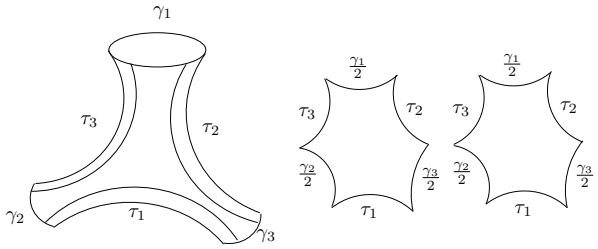

Figure 4. Topological pants and hyperbolic hexagons.

4.2. Canonical Segmentation

Suppose surface M has the uniformization hyperbolic metric $\bar{\mathbf{g}}$. In our work, we consider genus zero surfaces with multiple holes. First, we consider a topological disk with two holes inside, which we call a pair of *topological pants*, as shown in Figure 4. Let the boundary ∂M of M to be $\{\gamma_1, \gamma_2, \gamma_3\}$. Intuitively, γ_1 looks like the waist and the other two like trouser turnups. Then there exist three geodesics $\{\tau_1, \tau_2, \tau_3\}$, such that τ_i is perpendicular to both γ_j, γ_k. τ_ks partition the surface to 2 congruent hyperbolic hexagons, whose corner angles are all $90°$'s.

If the topology of the surface is more complicated, we need to decompose the surface to pairs of pants first in a canonical way. Suppose, there are n boundaries of the surface, $\partial M = \{\gamma_1, \gamma_2, \cdots, \gamma_n\}$, then we can use the following procedure to partition it to a sequence of pairs of pants. First, we find a loop γ surrounding both γ_1 and γ_2. Then according to the following theorem [26], there exists a unique geodesic homotopic to γ.

Theorem 4.1 *Suppose S is a surface with hyperbolic metric, then each homotopy class of S has a unique geodesic.*

We still denote that geodesic as γ. γ segments M to two parts, M_1 and M_2, M_1 is a pair of pants, M_2 has $n-1$ boundary components. By repeating this process, we can decompose M to $n-2$ pairs of pants.

4.3. Hyperbolic Hexagon Matching

We carried out the matching between both hyperbolic hexagons using harmonic mapping with feature correspondence constraints. It is known that if the target shape is convex, then the harmonic map is diffeomorphism. Since the hyperbolic hexagon is not convex, this step requires the usage of another hyperbolic space model, the *Klein model* [18]. In the Klein model, the hyperbolic hexagon is mapped to a convex Euclidean polygon with 6 sides, as shown in Figure 5.

The computation procedures for hyperbolic hexagon matching are:

1. Compute a hyperbolic mapping the $\phi_k : S_k \to D_k$.
2. Convert the Poincaré disk model to Klein model using Eqn. 4, then each hyperbolic hexagon becomes a convex polygon.
3. Let the corresponding feature points on S_k be $F_k = \{p_1^k, p_2^k, p_3^k, \cdots, p_m^k\}$. Compute a harmonic map $\tilde{f} : D_1 \to D_2$, such that $\Delta f = 0$, with the following constraints:
   (a) Feature constraints: $\tilde{f}(\phi_1(p_i^1)) = \phi_2(p_i^2), \forall p_i^k \in F_k$.
   (b) Boundary constraints: $\tilde{f}(\phi_1(\gamma_i^1)) = \phi_2(\gamma_i^2)$, if $\gamma_i^1 \in \partial S_1$ and $\gamma_i^2 \in \partial S_2$ are consistent.
4. The matching is given by $f = \phi_2^{-1} \circ \tilde{f} \circ \phi_1$.

The algorithm is applied on discrete meshes. The final mapping is represented as follows: Suppose $v \in S_1$ is a vertex on the first mesh, $f(v)$ is a point $p \in S_2$ on the second surface, and p is on a face $[v_1, v_2, v_3] \in S_2$, such that $p = \mu_1 v_1 + \mu_2 v_2 + \mu_3 v_3$, where (μ_1, μ_2, μ_3) are the barycentric coordinates of p in $[v_1, v_2, v_3]$. Then we represent $f(v)$ as a pair

$$f(v) = ([v_1, v_2, v_3], (\mu_1, \mu_2, \mu_3)), \tag{8}$$

and call it a *natural representation* of the matching f.

5. Experimental Results

In this section, we demonstrate the performance of our framework. This work handles 3D moving deformable data with complex topologies, which are very difficult to acquire. We thoroughly tested our algorithms on 30 facial scans with dynamic expressions, represented by the triangular meshes with about 15K vertices and 30K faces. The facial surfaces are topological two-hole annuli (both eye contours are difficult to detect accurately). These surfaces are representative because of their general topologies, with big distortions and very inconsistent boundaries. Such difficult experiments sufficiently support the generality and effectiveness of our method.

Matching and Registration for Dynamic Non-rigid 3D Faces Figures 6 and 7 illustrate our experimental results on matching two human faces with different expressions, acquired using the method described in [34] with greyscale texture. The feature points were computed directly using the SIFT [22] algorithm on the textures. We visualized the matching and registration results by consistent checkerboard texture mapping. It also shows that the intrinsic decompositions by geodesics are consistent between the 3D non-rigid faces to be matched.

Morphing by Registration Figure 7 shows the morphing between two 3D faces with large motion of eyes and significantly inconsistent boundaries.

Performance Comparison We compared our method with previous work [34, 20, 10] for 3D face matching and registration.

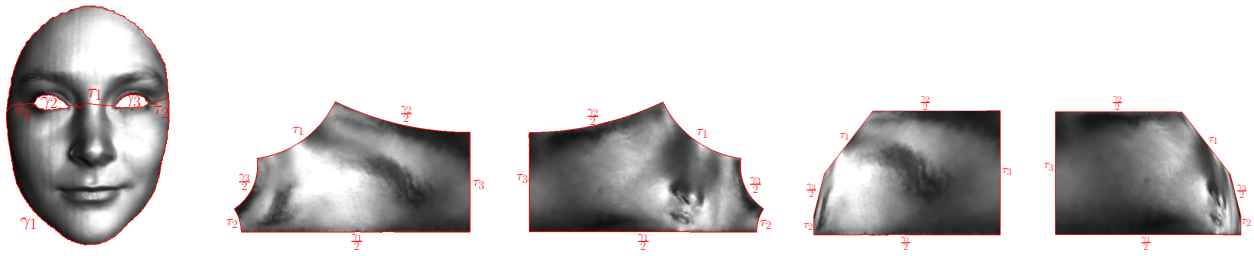

(a) Original Surface (b) Upper Poincaré (c) Lower Poincaré (d) Upper Klein (e) Lower Klein

Figure 5. Conversion from Poincaré hexagon to Klein hexagon.

Accuracy The matching accuracy is measured by registration error among Iterative Closest Point (ICP) [2], Euclidean Ricci Flow (ERF) [10] and Hyperbolic Ricci Flow (HRF) methods, see Table 1. First, we computed the registration error for facial surfaces by the relative Hausdorff average distance (RHAD) under rigid deformation (ICP), and non-rigid deformation (HRF). In detail, the distance error is the average distance between the source point and the corresponding image point, normalized by the diagonal of the bounding box of the target surface. As a baseline system, ICP is one of the most popular 3D shape matching method and has relatively good performance. All the tests demonstrate that HRF outperforms ICP. Then, we used the texture error in [10] for evaluation between both non-rigid deformations, ERF and HRF, see Table 1. The matching accuracy of the ERF method is highly sensitive to the choice of singularity.

Singularity The ERF method in [10] is the only previous method to compute the matching for multiple connected domains, but it often generates singularities which make the matching computation error-prone. The HRF method does not induce singularities. Intuitively, the *singularities* are those points whose neighborhood can not be flattened to the planar domain. For example, as shown in Figure 8, the ERF method has one singularity at the tip of nose, whose neighboring angles sum to 4π denoted by 8 right angles $\theta_1, \theta_2, ..., \theta_8$. At the same time, HRF makes the neighboring angles sum to 2π everywhere on the planar domain.

Discretization For surfaces with negative Euler number, the ERF method in [10] uses the singularity as the only landmark for domain decomposition to rectangle or trapezoid patches. The matching accuracy based on decomposition is directly determined by the choice of singularity. The HRF method uses the geodesics detected automatically to get hyperbolic hexagons. Such discretization is intrinsic and unique, and does not arouse the ambiguity.

Efficiency We implemented our algorithm using generic C++ on Windows XP and used conjugate gradient optimization for acceleration. Table 2 reports the computational time on a Laptop with CPU 2.00 GHZ, RAM 3.00 GB. Other mapping methods for computing such surfaces, like harmonic maps [34] and LSCMs [20], can not guarantee one-to-one maps and may generate intersections (see Figure 9), which depends on the prescribed points. The comparison among each mapping method is illustrated in Table 3.

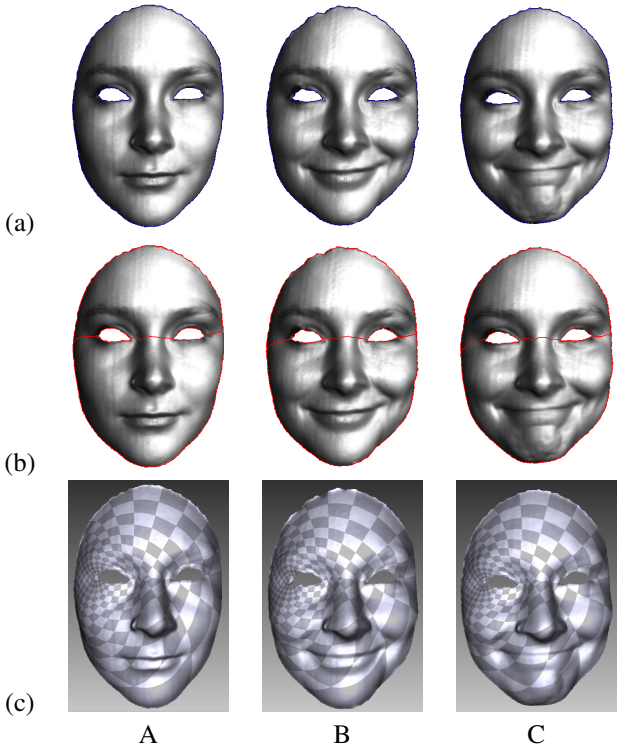

Figure 6. E1: Non-rigid matching and registration for 3D faces. (a) original surfaces A,B,C with expression change and mouth closed, which are genus zero with 2 holes. (b) the geodesics between each two boundaries corresponding to the hyperbolic lines on hyperbolic hexagons. (c) The registration results are visualized by different consistent checkerboard texture.

Automaticity The method is completely automatic. Given the target curvature, the hyperbolic mapping can be automatically and uniquely computed by Ricci flow till convergence. The canonical segmentation and pants decomposition are performed directly by automatic geodesic detection, which is unique and rigorous. The matching between each pair of hexagons with feature points is also automatic. If the open surface has n boundaries (including the outer boundary), then there are totally $n-2$ pairs of hyperbolic hexagons for matching.

Table 3. Performance comparison of geometric mapping methods.

	Harmonic Map	LSCM	Euclidean RF	Hyperbolic RF
Is one-to-one map	No	No	Yes	Yes
Time complexity	Linear	Linear	Non-linear	Non-Linear
Boundary occlusion	Sensitive	Not sensitive	Sensitive	Sensitive
Boundary constraint	Needed	Not Needed	Needed	Needed
Feature constraint	Not needed	Two points needed	Not Needed	Not Needed
Resolution change	Not sensitive	Not sensitive	Not sensitive	Not sensitive
Topology limited	Topological disk	Topological disk	Arbitrary surface	Arbitrary surface
Singularity	Yes	Yes	Yes	No

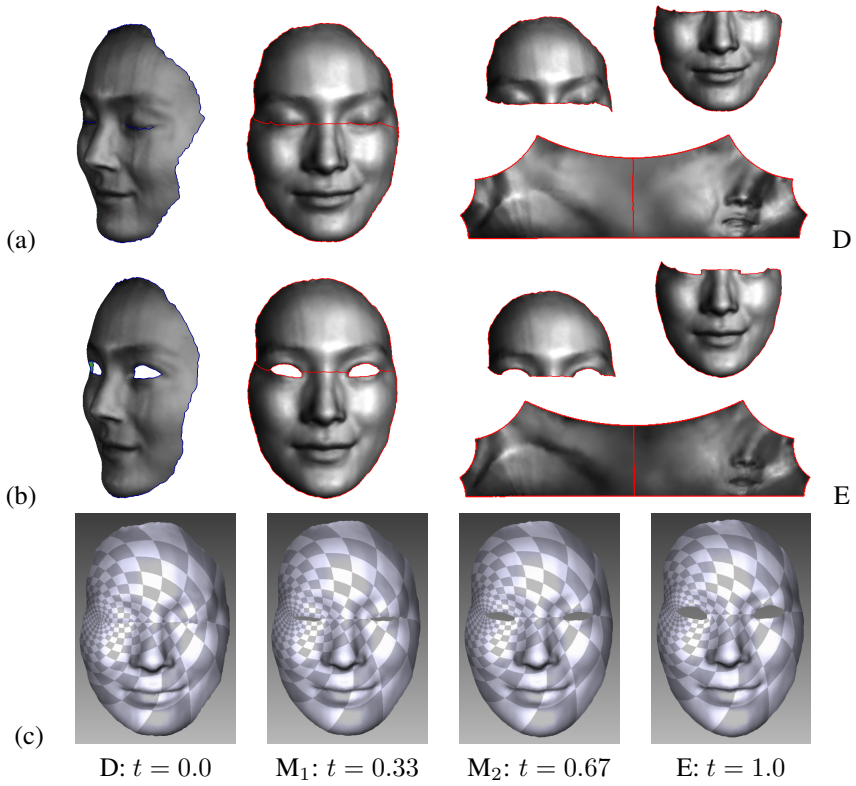

Figure 7. E2: Non-rigid morphing by registration. (a) and (b) are the two surfaces to be matched: (1) the original surfaces D, E with eye motion and inconsistent boundaries, (2) the traced geodesics, and (3) the hyperbolic mapping. (c) The morphing results M_1, M_2 with interpolation factors $t = 0.33, 0.67$ between D, E, visualized by consistent checkerboard texture mapping.

Table 1. Registration error under ICP, ERF and HRF methods.

Distance Error (%)	A-B	A-C	D-E
ICP	2.60	2.48	2.52
HRF	0.25	0.30	0.22
Texture Error (%)	A-B	A-C	D-E
ERF	4.03	4.06	8.24
HRF	4.05	4.11	8.13

Table 2. Computational time.

Name	A	B	C	D	E
Faces	28,800	28,759	28,820	13,671	13,461
Verts	14,743	14,733	14,767	6,983	6,865
HRF (s)	210	210	210	150	148

6. Conclusion

This paper proposes a novel 3D non-rigid face matching and registration method based on surface Hyperbolic Ricci Flow (HRF). For genus zero surfaces with multiple holes, the canonical hyperbolic metric is conformal to the original and can be efficiently computed by HRF. Through the intrinsic canonical segmentation, the surface can be decomposed to hyperbolic hexagons, which are easy for establishing surface matching. Hyperbolic Ricci flow induces diffeomorphisms between surfaces without singularity, and all the boundaries are intrinsically mapped to hyperbolic lines for alignment constraints. We demonstrate the generality and

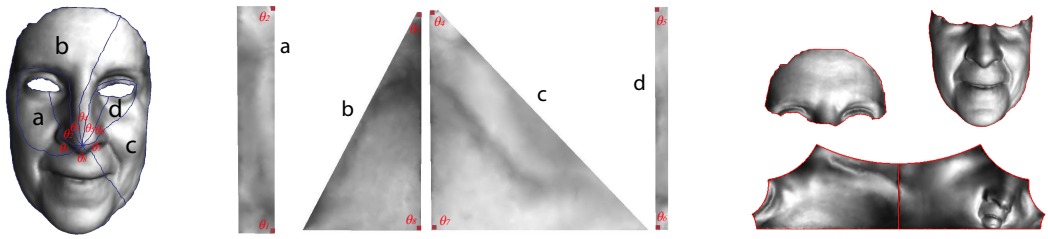

(a) (b) (c)

Figure 8. Singularity for Euclidean Ricci flow method. (a) The original surface with singularity at the tip of nose, where the surrounding angles are summed to 4π. (b) The mapping generated by Euclidean Ricci flow, where $\theta_1, \theta_2, ..., \theta_8$ correspond to right angles on the planar domain. (c) The Poincaré model generated by Hyperbolic Ricci flow method.

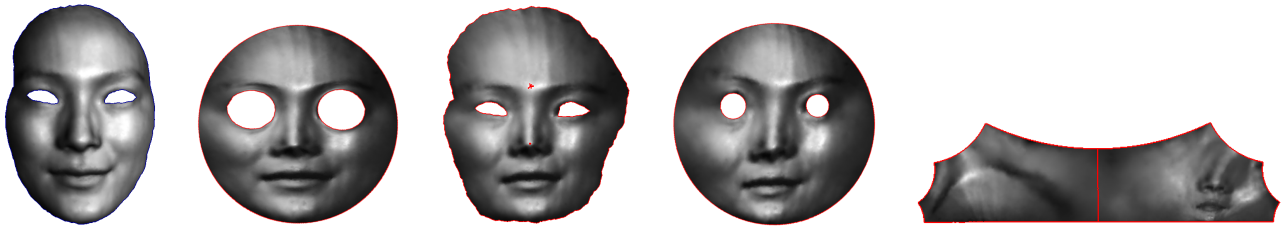

(a) Original Surface (b) Harmonic Map (c) Least-Square Conformal Map (d) Euclidean Ricci Flow (e) Hyperbolic Ricci Flow

Figure 9. Comparison of geometric mappings for multiply connected domains. (b) HM makes the boundary areas much stretched to degenerated triangles. (c) LSCM needs two feature points, here labeled at the brow and the tip of nose. (d) and (e) are one-to-one and onto.

flexibility of this intrinsic shape representation for 3D human face matching and registration by various experiments. In future work, we will continue to explore properties of Ricci flow maps and reduce computational complexity. We also plan to apply our method for applications such as 3D object classification and recognition.

References

[1] M. M. B. Alexander M. Bronstein and R. Kimmel. Expression-invariant representations of faces. *IEEE Trans. on Image Processing*, 16(1):188–197, 2007.

[2] P. J. Besl and N. D. McKay. A method for registration of 3-D shapes. *IEEE Trans. Pattern Anal. Mach. Intell.*, 14(2):239–256, 1992.

[3] A. M. Bronstein, M. M. Bronstein, and R. Kimmel. Expression-invariant representations of faces. *IEEE Trans. Image Processing*, 16(1):188–197, 2007.

[4] A. M. Bronstein, M. M. Bronstein, and R. Kimmel. Rock, paper, and scissors: extrinsic vs. intrinsic similarity of non-rigid shapes. In *ICCV*, 2007.

[5] R. Campbell and P. Flynn. A survey of free-form object representation and recognition techniques. *Computer Vision and Image Understanding*, 81:166–210, 2001.

[6] B. Chow and F. Luo. Combinatorial ricci flows on surfaces. *Journal Differential Geometry*, 63(1):97–129, 2003.

[7] P. Dalal, B. C. Munsell, S. Wang, J. Tang, K. Oliver, H. Ninomiya, X. Zhou, and H. Fujita. A fast 3d correspondence method for statistical shape modeling. In *CVPR*, 2007.

[8] A. Frome, D. Huber, R. Kolluri, T. Bulow, and J. Malik. Recognizing objects in range data using regional point descriptors. In *ECCV*, May 2004.

[9] T. Funkhouser, P. Min, M. Kazhdan, J. Chen, A. Halderman, D. Dobkin, and D. Jacobs. A search engine for 3d models. In *ACM TOG*, pages 83–105, 2003.

[10] X. Gu, S. Wang, J. Kim, Y. Zeng, Y. Wang, H. Qin, and D. Samaras. Ricci flow for 3d sahpe analysis. In *ICCV*, 2007.

[11] X. Gu, Y. Wang, T. F. Chan, P. M. Thompson, and S. Yaun. Genus zero surface conformal mapping and its application to brain surface mapping. *TMI*, 23(7), 2004.

[12] X. Gu and S.-T. Yau. Global conformal parameterization. In *SGP*, pages 127–137, 2003.

[13] R. Hamilton. The ricci flow on surfaces. *Mathematics and General Relativity*, 71:237–262, 1988.

[14] X. Huang, N. Paragios, and D. Metaxas. Establishing local correspondences towards compact representations of anatomical structures. In *MICCAI'03*, pages 926–934, 2003.

[15] D. Huber, A. Kapuria, R. Donamukkala, and M. Hebert. Parts-based 3d object classification. In *CVPR*, pages II: 82–89, June 2004.

[16] M. Jin, J. Kim, and X. Gu. Discrete surface ricci flow: Theory and applications. In *IMA Conference on the Mathematics of Surfaces*, pages 209–232, 2007.

[17] M. Jin, J. Kim, F. Luo, S. Lee, and X. Gu. Conformal surface parameterization using euclidean ricci flow. Technique report, May 2006.

[18] M. Jin, F. Luo, and X. Gu. Computing surface hyperbolic structure and real projective structure. In *SPM '06: Proceedings of the 2006 ACM symposium on Solid and physical modeling*, pages 105–116, New York, NY, USA, 2006. ACM Press.

[19] L. Kharevych, B. Springborn, and P. Schröder. Discrete conformal mappings via circle patterns. *ACM Trans. Graph.*, 25(2):412–438, 2006.

[20] B. Levy, S. Petitjean, N. Ray, and J. Maillot. Least squares conformal maps for automatic texture atlas generation. In *SIGGRAPH02*, pages 362–371, 2002.

[21] W.-Y. Lin, K.-C. Wong, N. Boston, and H.-H. Yu. Fusion of summation invariants in 3d human face recognition. In *CVPR*, 2006.

[22] D. Lowe. Object recognition from local scale-invariant features. In *ICCV*, pages 1150–1157, 1999.

[23] R. Malladi, J. A. Sethian, and B. C. Vemuri. A fast level set based algorithm for topology-independent shape modeling. *JMIV*, 6(2/3):269–290, 1996.

[24] R. Osada, T. Funkhouser, B. Chazelle, and D. Dobkin. Shape distributions. In *ACM TOG*, volume 21, pages 807–832, 2002.

[25] S. Ruiz-Correa, L. Shapiro, and M. Meila. A new paradigm for recognizing 3d object shapes from range data. In *ICCV*, pages 1126–1133, 2003.

[26] M. Seppala and T.S. *Geometry of Riemann Surfaces and Teichmuller Spaces*. North-Holland Math Stud., 1992.

[27] E. Sharon and D. Mumford. 2d-shape analysis using conformal mapping. In *CVPR*, pages II: 350–357, 2004.

[28] J. Starck and A. Hilton. Correspondence labelling for wide-timeframe free-form surface matching. In *ICCV*, 2007.

[29] Y. Sun and M. Abidi. Surface matching by 3d point's fingerprint. In *ICCV*, pages II: 263–269, 2001.

[30] D. Terzopoulos, A. Witkin, and M. Kass. Constraints on deformable models: Recovering 3d shape and nonrigid motion. *Artificial Intelligence*, 35:91–123, 1988.

[31] B. Vemuri, A. Mitiche, and J. Aggarwal. Curvature-based representation of objects from range data. *Image and Vision Computing*, 4:107–114, 1986.

[32] S. Wang, Y. Wang, M. Jin, X. D. Gu, and D. Samaras. Conformal geometry and its applications on 3d shape matching, recognition, and stitching. *PAMI*, 29(7):1209 – 1220, 2007.

[33] Y. Wang, M.-C. Chiang, and P. M. Thompson. Mutual information-based 3d surface matching with applications to face recognition and brain mapping. *ICCV05*, 1:527–534, 2005.

[34] Y. Wang, M. Gupta, S. Zhang, S. Wang, X. Gu, D. Samaras, and P. Huang. High resolution tracking of non-rigid 3d motion of densely sampled data using harmonic maps. In *ICCV*, pages I: 388–395, 2005.

[35] J. Wyngaerd, L. Gool, R. Koch, and M. Proesmans. Invariant-based registration of surface patches. In *ICCV*, pages 301–306, 1999.

[36] P. Xiao, N. Barnes, T. Caetano, and P. Lieby. An mrf and gaussian curvature based shape representation for shape matching. In *CVPR*, 2007.

[37] D. Zhang and M. Hebert. Harmonic maps and their applications in surface matching. In *CVPR*, pages II: 524–530, 1999.